JOURNAL OF AIRCRAFT
Vol. 48, No. 4, July–August 2011

Advanced Sonic Boom Prediction Using the Augmented Burgers Equation

Sriram K. Rallabhandi*
National Institute of Aerospace, Hampton, Virginia 23666

DOI: 10.2514/1.C031248

This paper presents an approach to predict the sonic boom ground signatures accurately by numerically solving the augmented Burgers equation entirely in the time domain. The method is capable of predicting the shock thicknesses, thus improving the frequency spectrum of the ground signatures. This also improves the loudness calculation when compared with linear theory methods, because the shock rise times are computed and not empirically adjusted or corrected. The method is capable of predicting undertrack and offtrack ground signatures, with or without wind effects, along with consideration for aircraft maneuvers. This method is very efficient and accurate, making it a very useful design tool in the development of supersonic cruise aircraft.

Nomenclature

A	=	ray tube area, m^2
A_h	=	horizontal component of ray tube area, m^2
$\mathbf{c}$	=	ray tube trajectory
C_ν	=	dimensionless dispersion
c_0	=	ambient speed of sound, m/s
l	=	ξ-direction cosine
M	=	Mach number
m_ν	=	dispersion parameter
n	=	Z-direction cosine
$\mathbf{n}$	=	unit vector along ray path direction
P	=	dimensionless pressure
p_0	=	reference pressure
s	=	distance measured along ray path, m
t	=	time coordinate, s
TR	=	shock rise time, s
t'	=	retarded time
u	=	wind components in ξ direction, m/s
v	=	wind components in η direction, m/s
$\mathbf{W}$	=	wind vector
$\mathbf{x}$	=	shock formation distance
$x; y; z$	=	Cartesian coordinates of ray paths
α_0^{tv}	=	thermoviscous attenuation coefficient
β	=	$1 + [(\gamma - 1)/2]$
Γ	=	dimensionless thermoviscous parameter
γ	=	angle-defining wave normal plane
δ	=	diffusing parameter
η	=	coordinate perpendicular to wave normal direction
θ	=	wave normal inclinations to horizontal plane
θ_ν	=	dimensionless relaxation time parameter
ξ	=	coordinate aligned with wave normal direction
ρ	=	atmospheric density
σ	=	nondimensional distance
τ	=	dimensionless time
τ_ν	=	dimensionless time for each relaxation mode
ϕ	=	azimuthal angle
ω_0	=	angular frequency

Received 23 September 2010; revision received 28 November 2010; accepted for publication 28 November 2010.

*Research Scientist II.

I. Introduction

SUPERSONIC flight's biggest challenge remains mitigation of sonic boom to levels where the noise footprint from supersonic cruise is considered acceptable to humans and building structures. Sonic boom prediction tools have been around since the 1960s. Most of the numerical methods developed during the earlier phases of commercial supersonic aircraft research were based on the linear theory concepts laid out originally by Whitham [1] and later by Hayes [2]. The initial computer programs [3,4] rested heavily on this theory. Several new codes have come about in later years (PCBOOM [5], for example), but the underlying physics of boom propagation was based on linear and weak shock theory given by Whitham [1]. Since the prediction was based on linear theory, the sonic boom minimization theory, originally proposed by Seebass and George [6] and later extended by several others [7–11], has also been based on linear theory. However, the main drawback of linear theory and weak shock assumption is its inability to predict the shock rise times. The predicted ground signatures using traditional approaches represent the shocks as discontinuous jumps. However, during the calculation of the frequency spectrum and, subsequently, the noise metrics (most importantly perceived loudness), one has to resort to empirical or numerical shock thickening to quantify and compare the impact of ground signatures. This shock thickening is essential, because fast Fourier transforms (FFT) and other numerical techniques, required in the computation of any loudness metric, cannot be applied to waveforms with shock discontinuities. The shock thickening process is prone to error, because rise times calculated by this process are heavily dependent on the empirical or numerical factors chosen for converting the discontinuous shocks into continuous profiles. Furthermore, there is the unanswered question with regard to shock merging: namely, if two shocks are close by in the predicted ground signature, when should they be merged into a single shock during the thickening process? A common solution to this depends on the parameters chosen by the designer. Unfortunately, shock thickening and merging processes produce loudness and other noise metrics that may not be accurate. During optimization exercises, it is the tendency of the optimizer to exploit the shock merging process to its advantage. This is problematic, because the optimized loudness values may not be as optimistic as the optimizer believes they are.

To overcome these problems, several researchers in the past [12–14] have looked at boom prediction methods that calculate the rise times without resorting to weak shock theory and area balancing techniques. These methods are based on solutions to the augmented Burgers equation. In essence, the regular Burgers equation is augmented with absorption, molecular relaxation, atmospheric stratification, and spreading terms, in addition to the nonlinear term from the regular equation. Some methods [12–14] have used time domain to perform nonlinear corrections to the pressure waveform during propagation, and some have used the frequency domain to

account for the dissipation and relaxation. Frequent conversion from time domain to frequency domain and back during atmospheric propagation may allow numerical errors to creep in. Even if the numerical errors can be bounded, frequent FFT and inverse FFT operations add an additional overhead during the propagation process. To overcome these issues, the current work uses a time domain algorithm to account for all the propagation mechanisms and is an extension of the algorithm presented by Cleveland [13]. The extensions are as follows:

1) The first extension is the ability to handle different input waveforms: either an offbody dp/p pressure waveform or an F function generated, perhaps from boom minimization theory or an equivalent area distribution used in design exercises [15].

2) The second extension is the ability to predict ground signatures in the presence of horizontally stratified wind profiles.

3) The third extension is the ability to handle nonstandard atmospheres if needed. In this case, users can provide temperature, wind, and relative humidity distributions.

4) The fourth extension is the prediction of offtrack signatures.

5) The fifth extension is the prediction of ground intersection location with respect to the aircraft location, as well as time taken for the pressure disturbance to reach the ground.

Several other extensions useful in the design process are likely in the future. These include the addition of logic to take care of focused booms and postprocessing using a turbulence filter to simulate the passage of the waveform through a slab of turbulence. The name given to the sonic boom prediction code developed in this study is sBOOM.

II. Sonic Boom Prediction

This section briefly describes the technical details used in the boom propagation process of sBOOM. As has been mentioned in the previous section, the heart of this program uses the augmented Burgers equation, given in Eq. (1), that considers effects such as nonlinearity, thermoviscous absorption, and any number of molecular relaxation phenomena during the propagation of waveforms through the atmosphere. This equation may be converted to dimensionless form, as shown in Eq. (2), with additional terms resulting from geometrical spreading and propagation through stratified atmosphere:

$$\frac{\partial p}{\partial x} = \frac{\beta p}{\rho_0 c_0^3}\frac{\partial p}{\partial t'} + \frac{\delta}{2c_0^3}\frac{\partial^2 p}{\partial t'^2} + \sum_\nu \frac{c_\nu'}{c_0^2}\int_{-\infty}^{t'} \frac{\partial^2 p}{\partial y^2} e^{-(t'-y)/t_\nu}\,\mathrm{d}y \tag{1}$$

$$\frac{\partial P}{\partial \sigma} = P\frac{\partial P}{\partial \tau} + \frac{1}{\Gamma}\frac{\partial^2 P}{\partial \tau^2} + \sum_\nu C_\nu \frac{\partial^2/\partial\tau^2}{1+\theta_\nu(\partial/\partial\tau)}P - \frac{\partial A/\partial A}{2A}P + \frac{[\partial(\rho_0 c_0)]/\partial\sigma}{2\rho_0 c_0}P \tag{2}$$

Here, $P(\sigma,\tau) = p/p_0$, where p_0 is a reference pressure. The nondimensional distance is given by $\sigma = x/\bar{x}$, where $\mathbf{x} = \rho_0 c_0^3/\beta\omega_0 p_0$ is the shock formation distance of a plane wave with peak pressure p_0, ambient density ρ_0, and angular frequency ω_0, with $\beta = 1 + [(\gamma - 1)/2]$ being the coefficient of nonlinearity. The dimensionless time τ is defined as $\tau = \omega_0 t'$, where t' is the retarded time coordinate. The dimensionless thermoviscous parameter is denoted by Γ and defined as $\Gamma = 1/\alpha_0^{\mathrm{tv}}\bar{x}$, where the thermoviscous attenuation coefficient is given by $\alpha_0^{\mathrm{tv}} = \delta\omega_0^2/2c_0^3$, with δ being the diffusion parameter. The variable θ_ν is a dimensionless relaxation time parameter given by $\theta_\nu = \omega_0 t_\nu$. The dimensionless dispersion parameterC_ν is given by $C_\nu = (m_\nu \tau_\nu \omega_0^2/2c_0)\bar{x}$, where m_ν is the dispersion parameter, a function of the equilibrium and frozen sound speeds in a particular medium, and τ_ν is the dimensionless time for each relaxation mode. Equation (2) represents the dimensionless equation that is numerically solved by sBOOM.

The numerical solution strategy is to use an operator splitting method wherein the individual mechanisms of wave propagation are solved independently and successively over incremental steps $\Delta\sigma$. When the step size is chosen to be small, the combination of the independent solutions of the different propagation mechanisms theoretically matches the solution of the whole equation. The solution process involves discretization of the original input waveform into a desired uniform spacing grid. A nonuniform grid was tested as well; however, it adds to the overhead without adding much to the results. All the results presented in this study use a uniform grid for discretization. Finite difference approximations are used to numerically solve each of the equations over successive steps. Other details pertaining to the solution strategy are provided by Cleveland [13], and the interested reader may refer to that for additional details regarding the solution methodology.

III. Ray Tracing

Wave propagation through the atmosphere is carried out using geometric acoustics and ray tracing. Several previous studies have documented the ray tracing aspect during boom propagation to the ground, without winds [16,17] as well as with winds [14,18–20]. In this work, the ray paths are calculated in the wave normal reference frame following Onyeonwu [18]. The sketch showing the initial wave normal orientation relative to wind is shown in Fig. 1. Given the flight conditions M and the azimuthal angle ϕ, the relevant wave normal plane orientation angles may be computed easily. Particularly, the planar angle defining the wave normal plane γ and the wave normal inclination angle with respect to the horizontal θ are given by Eq. (3). The wind velocity components are projected parallel ξ and perpendicular η to the wave normal plane based on the flight heading angle, the wind blowing angle, and the initial wave normal orientation:

$$\sin\gamma = \lambda\sin\phi[1 + \lambda^2\sin^2\phi]^{-1/2} \tag{3}$$

$$\cos\theta = -\frac{1}{M\cos\gamma}$$

where

$$\lambda = (M^2 - 1)^{-1/2}$$

The ray propagation equations [18] are shown in Eq. (4) for the sake of completeness. In this equation, $l = \cos\theta$ and $n = \sin\theta$ are direction cosines in the ξ and z directions, respectively. Speed of sound in the atmosphere c_0, wind components in the ξ,η frame (u, v), the ray path distance s, as well as the time coordinate t, are included in these equations:

$$\frac{\mathrm{d}\xi}{\mathrm{d}z} = \frac{(lc_0 + u)}{nc_0}, \qquad \frac{\mathrm{d}\eta}{\mathrm{d}z} = \frac{v}{nc_0}, \qquad \frac{\mathrm{d}t}{\mathrm{d}z} = \frac{1}{nc_0}$$
$$\frac{\mathrm{d}s}{\mathrm{d}z} = \left[\frac{\mathrm{d}\xi^2}{\mathrm{d}z} + \frac{\mathrm{d}\eta^2}{\mathrm{d}z} + 1\right]^{1/2} \tag{4}$$

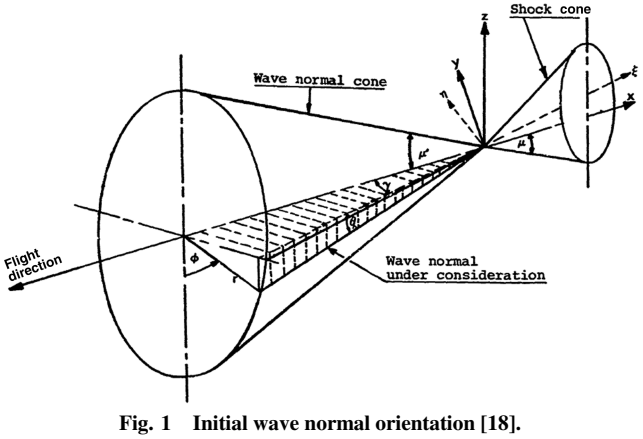

Fig. 1 Initial wave normal orientation [18].

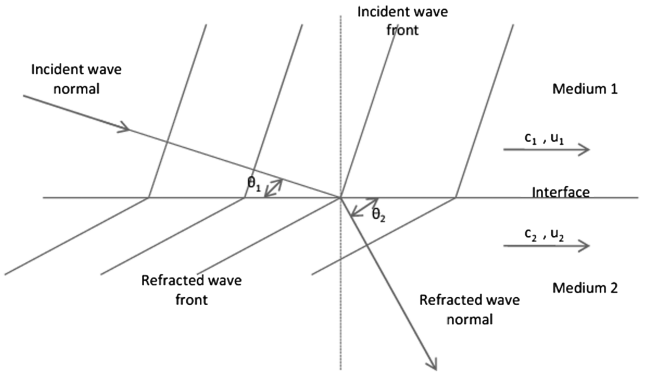

Fig. 2 Refraction via Snell's law [18].

As the signature propagates from the aircraft altitude toward the ground, geometric acoustics principles, similar to the principles of optics, may be applied. Because of the presence of atmospheric sound speed gradients, refraction of the incident normals occurs according to Snell's law. This is depicted in Fig. 2 in the presence of winds. Equation (5) presents this law for numerical implementation. When the aircraft heading is different, this equation needs to be modified accordingly:

$$\frac{c_1}{\cos\theta_1} + u_1 = \frac{c_2}{\cos\theta_2} + u_2 \tag{5}$$

Equations (4) are used to define the ray paths in the ξ, η plane. These are then projected into the Cartesian x, y, z plane according to a simple coordinate transformation given in Eq. (6):

$$x = \xi\cos\gamma - \eta\sin\gamma, \qquad y = \xi\sin\gamma + \eta\cos\gamma \tag{6}$$

Equations (4) are used to calculate the ray paths at different times during the propagation process. Equations (6) are then used to transform the locations to the x-y plane. This procedure is implemented for four different rays, thus forming a ray tube, according to the ray theory of boom propagation. The horizontal area of the ray tube A_h is calculated as the cross product of the location vectors of the adjacent rays in the ray tube emanating from the aircraft. The actual ray tube area A perpendicular to the wavefront is then calculated according to Eq. (7), where the wind vector **W** and the unit vector representing the ray path direction **n** are included. The ray path direction is obtained from the ray tube trajectory **c** given in Eq. (8):

$$A = \frac{cA_h\sin\theta}{c_n} \tag{7}$$

where

$$c_n = c + \mathbf{W}.\mathbf{n}$$

$$\mathbf{c} = c\mathbf{n} + \mathbf{W} \tag{8}$$

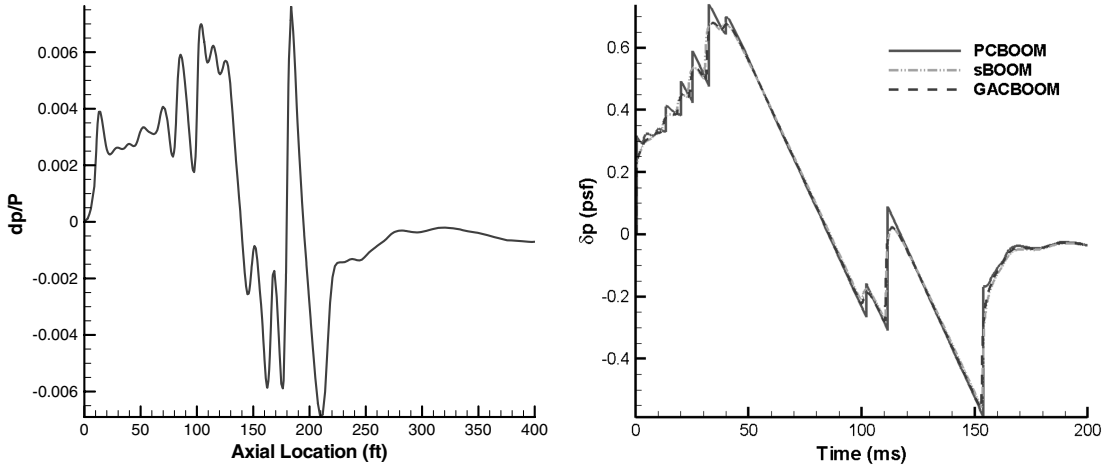

a) Near-field pressure distribution **b) Ground signature comparison**

Fig. 3 Comparison of ground signatures for an aircraft.

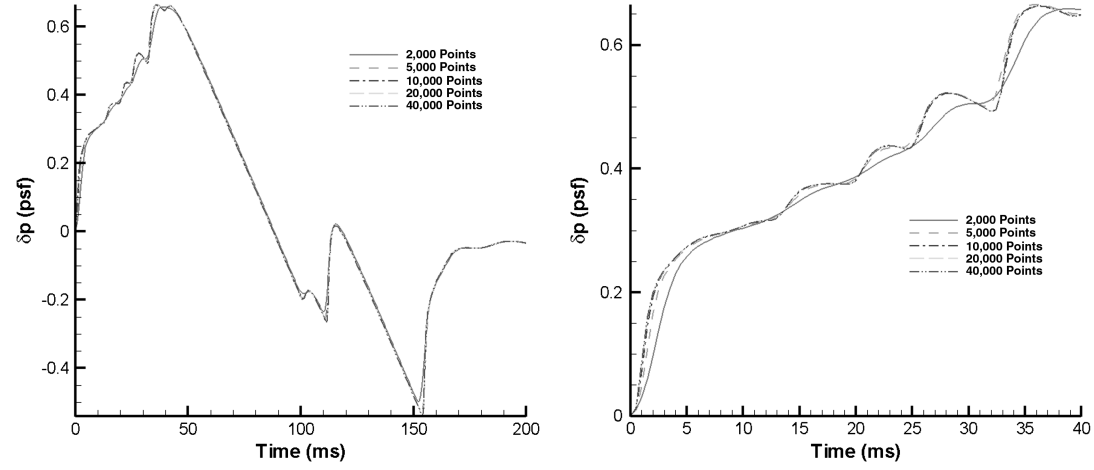

a) Ground signature sensitivity to sampling rate **b) Ground signature sensitivity to sampling rate - close up**

Fig. 4 Ground signature sensitivity to sampling rate.

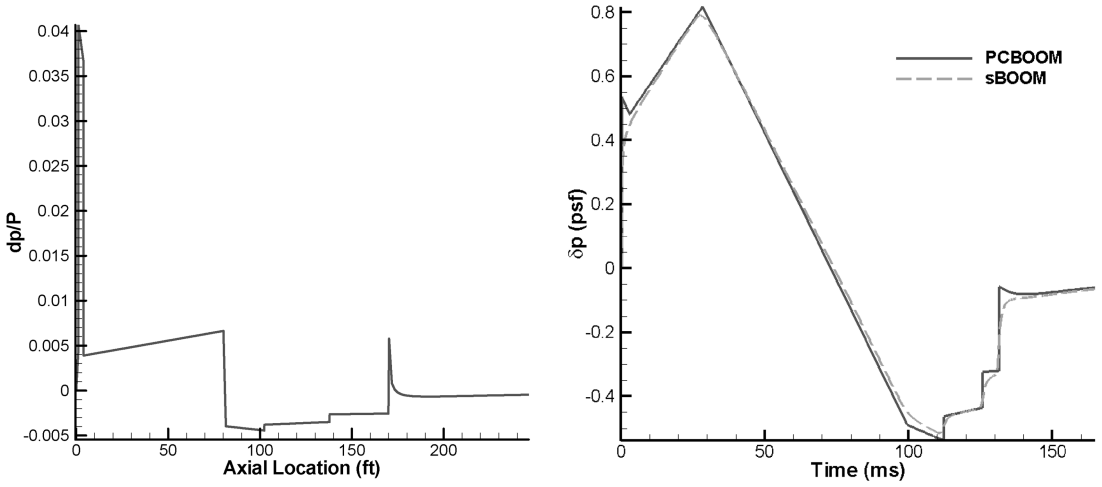

a) Target near-field pressure distribution b) Ground signature comparison

Fig. 5 Comparison of ground signatures for a boom minimization form.

Finally, during the propagation process, the Blokhintzev invariant [4,20] is maintained to update the magnitude of the pressure waveform based on the ray tube areas, speed of sound, and atmospheric density ρ. In the presence of winds, this is given by Eq. (9):

$$p\sqrt{\frac{c_n^2 A}{\rho c^3}} = \text{constant} \tag{9}$$

IV. Results, Validation, and Discussion

This section provides and discusses the ground signatures obtained for a couple of starting waveforms. The predicted sonic boom ground signatures are compared against existing tools for the sake of validating the current method. The first comparison is for an aircraft concept for which the offbody pressure distribution at three body lengths is obtained from a stretched-grid computational fluid dynamics (CFD) run [15,21] using USM3D [22] and is given in Fig. 3a. When transferring the CFD near field to sBOOM for

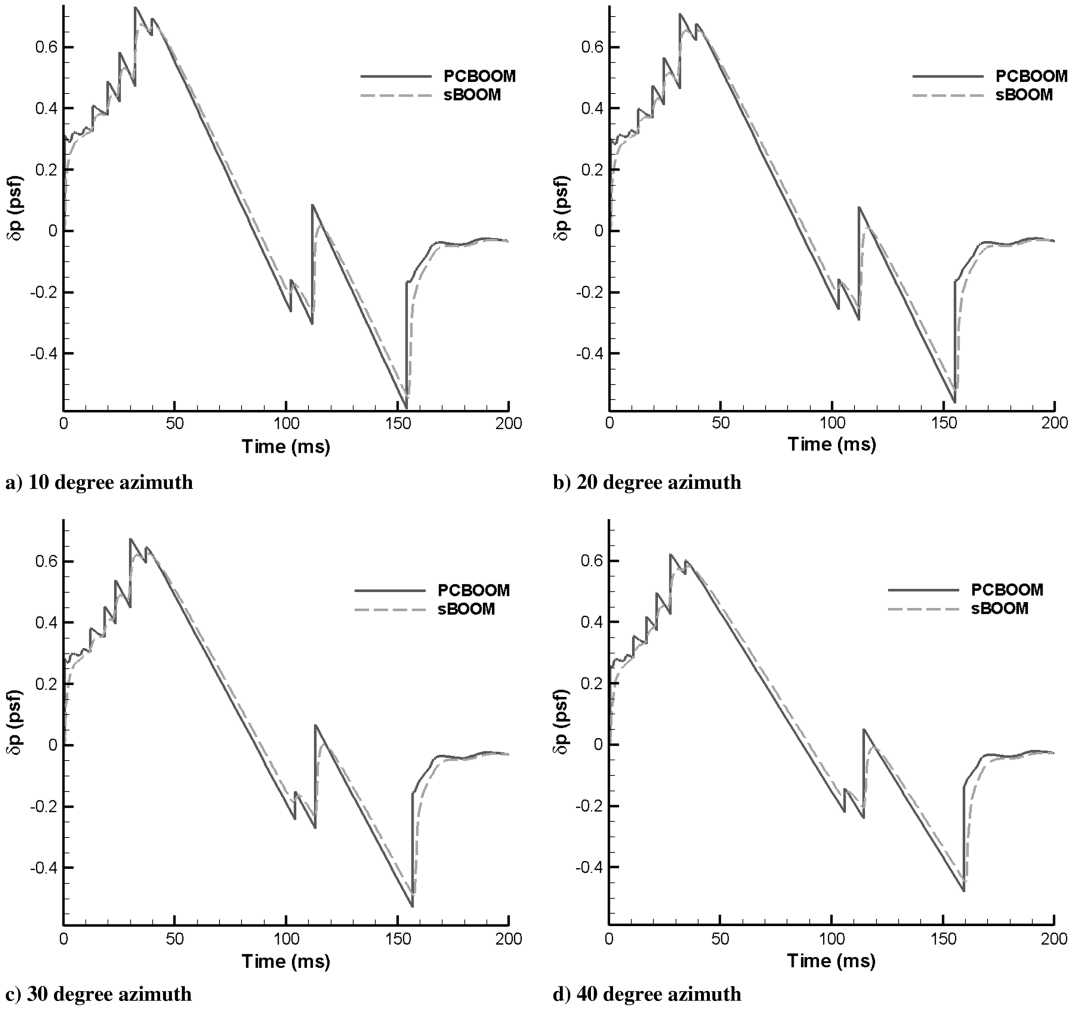

a) 10 degree azimuth b) 20 degree azimuth

c) 30 degree azimuth d) 40 degree azimuth

Fig. 6 Comparison of offtrack ground signatures.

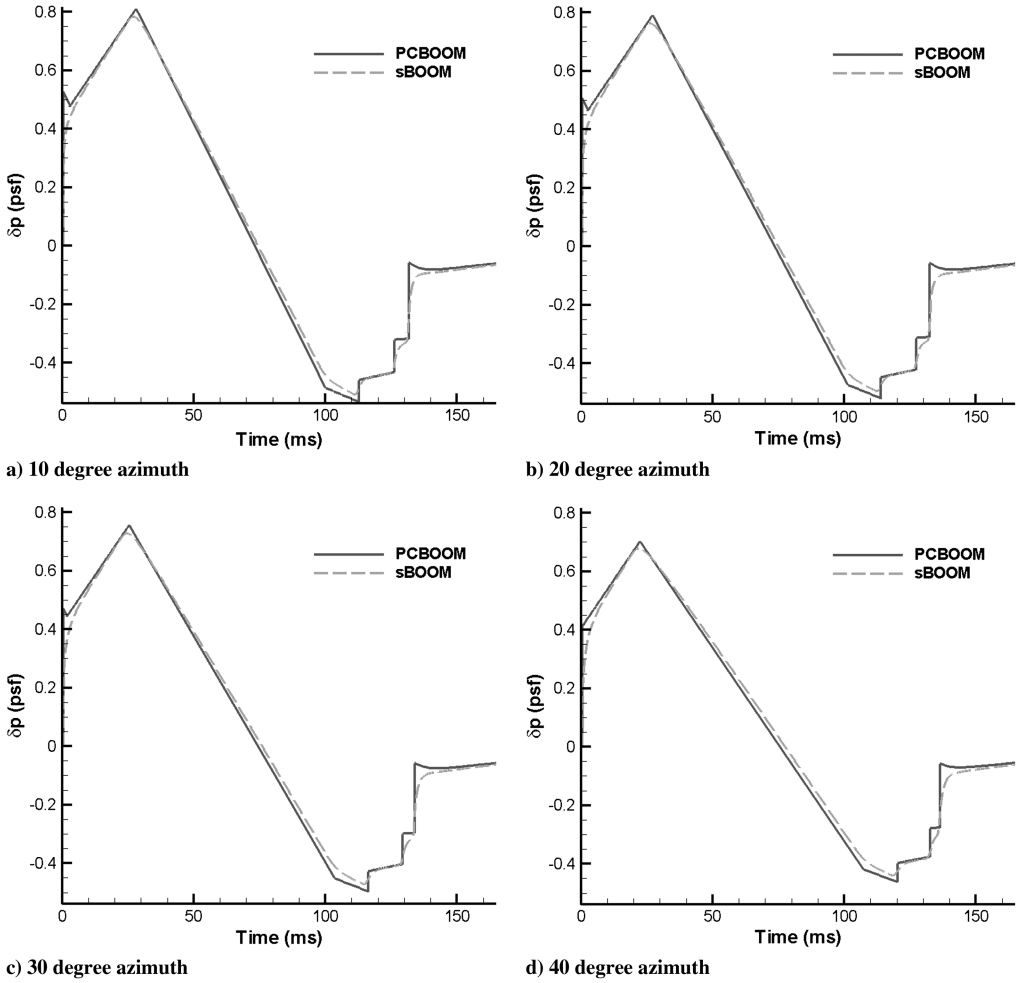

Fig. 7 Comparison of offtrack ground signatures for a boom minimization form.

propagation, both linear and quadratic interpolation techniques were tried. However, the ground signatures and loudness values were almost identical. Therefore, in all the plots shown in this paper, CFD near-field waveforms are linearly interpolated to generate input for sBOOM propagation. The cruise altitude is 15,742.92 m (51,650 ft), and the cruise Mach number is 1.8. Figure 3b shows the comparison of the sBOOM undertrack ground signature with that from PCBOOM. Comparison is also shown against a Gulfstream version of the Burgers equation propagation code GACBOOM. The sBOOM output matches well with GACBOOM output, while both the Burgers propagation codes match well to PCBOOM in terms of shock locations. The code sBOOM can predict the rise times for the shocks: a feature absent in PCBOOM signatures. Because of the empirical rise time calculation, the perceived loudness calculated using PCBOOM is 86.8 PLdB (perceived loudness level in decibels) [23], as opposed to a value of 90.5 PLdB using sBOOM or GACBOOM. These loudness values are counterintuitive at first, because ground signatures from sBOOM have rounded peaks and longer rise times than those from PCBOOM. Hence, the loudness values should be lower compared with PCBOOM. However, since PCBOOM cannot predict shock rise times, loudness results from PCBOOM are obtained using empirical modifications to the rise time using the hyperbolic tangent shock structure with a rise time of 3 ms for each pounds-per-square-foot change in the ground pressure compared with ambient. Mathematically, the rise time is given by $\mathrm{TR} = 0.003/\Delta p$ psf [20,24]. This factor, based on flight-test measurements to account for cumulative atmospheric effects, causes loudness values to be smaller than sBOOM. However, this correction factor is based on large aircraft, such as the high-speed civil transport, and is perhaps not directly applicable to business jets with shaped ground signatures. Any optimization study using perceived loudness values as one of the objectives may cause the results to be too optimistic if empirical shock thickening methods are used.

The sampling rate used during the propagation process has an impact on the propagation results. To study this effect, a convergence exercise was carried out with varying sampling rates. The results are shown in Fig. 4a. A close-up of the front part of the ground signatures is shown in Fig. 4b. It is seen that too few sampling points cause the ground signatures to not be fully developed. All signatures with sampling points beyond 10,000 converged to the same ground signature, not only for this case but for several other cases tested. All the results presented in this work use 20,000 sampling points for atmospheric propagation.

Generation of suitable targets for inverse design purposes is also a useful exercise in the supersonic design process. Therefore, the second case shown here compares the undertrack signatures obtained by propagating a target near field, shown in Fig. 5a. The target distribution is obtained using an F-function parameterization strategy based on the extensions to the sonic boom minimization theory, as given by Plotkin et al. [11]. The ground signature comparison is shown in Fig. 5b. It is seen that the shock locations and amplitudes match well; the sBOOM signatures are smooth and

Table 1 Arbitrary wind distribution

Altitude, m)	X wind, m/s	Y wind, m/s
0	25.0	−50.0
5,000.0	40.0	−80.0
10,000.0	60.0	−120.0
20,000.0	80.0	−160.0

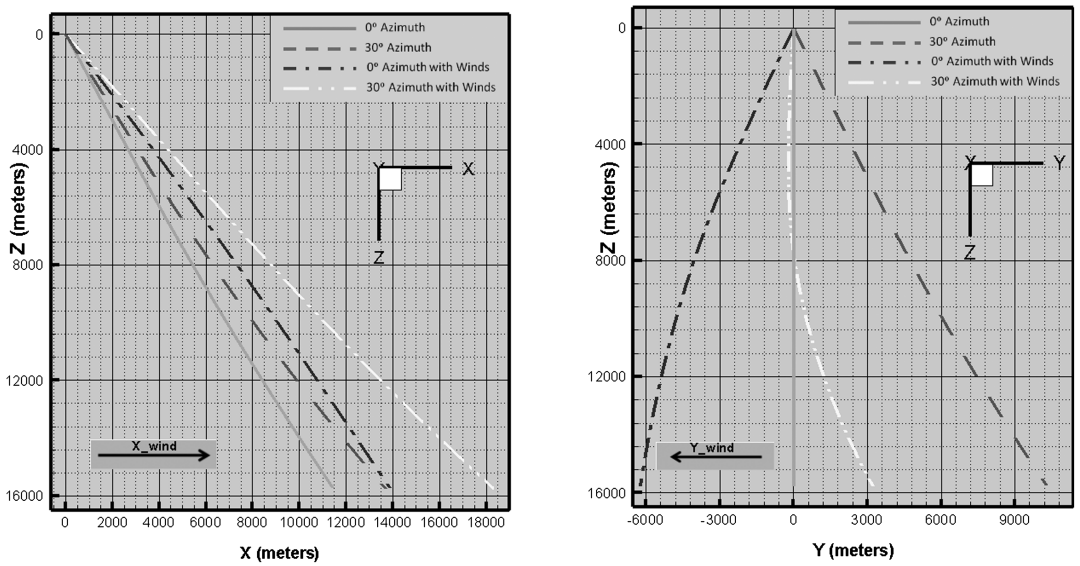

Fig. 8 Ray paths with and without wind.

rounded off, while the PCBOOM signatures display the shock jump discontinuity.

Comparisons of the ground signatures at offtrack azimuthal angles are given next. Offtrack signatures are important from a design perspective and, therefore, should be considered as well. Figures 6 and 7 compare the PCBOOM and sBOOM signatures at different azimuthal angles for the two near fields discussed previously. From these figures, one can observe that there is good agreement between the two codes. The sBOOM code has the additional benefit that loudness values are based on computed analytical rise times rather than empirical corrections and, perhaps, may be used more effectively in optimization and design exercises.

Sonic boom ground signatures vary greatly based on the prevalent wind conditions. To study the effect of winds, an arbitrary wind distribution, given in Table 1, was used to measure the impact on the sonic boom ground signatures calculated at the ground. A negative sign for the wind in the Y direction indicates that the wind is blowing away from the origin in the negative Y-axis direction.

A. Effect of Winds on Ray Paths

Depending on the direction of the winds, the ray paths from the aircraft cruise altitude to the ground are changed. Assume, for the sake of argument, that the wind distribution is as given in Table 1. Assume that a near-field pressure distribution (Fig. 3a) is propagated to the ground and undertrack, and offtrack (azimuth $= 30°$) signatures are calculated with and without winds using the same cruise flight conditions specified at the beginning of this section, with a heading angle of 0° (but flying with the wind component at an altitude added to the vehicle's ground velocity). The aircraft heading angle is the angle between the direction of flight and the X axis (east). Thus, a value of 180° would mean the flight direction is along the negative X axis, and a value of 90° would mean the flight direction is along the negative Y axis (north).

The ray paths for these cases are plotted in Fig. 8. From the figure, it is seen that, for no-wind cases, ray path distances are much longer, as expected, for offtrack computations compared with undertrack computations. This allows additional evolution time for the pressure profile before it reaches the ground. In cases where the undertrack profile is fully evolved, offtrack ray paths allow a mechanism for attenuation of the signatures. For example, if an aircraft produces an N-wave undertrack, then the offtrack profiles will be attenuated with respect to the undertrack. However, for shaped undertrack ground signatures, longer offtrack ray paths allow for additional shock coalescence (nonlinearities), in addition to the attenuation mechanisms, in the form of absorption and relaxation. Thus, for shaped undertrack ground signatures, the offtrack signatures might be larger in magnitude than the undertrack signatures and possibly have higher frequency content that can increase the loudness compared with the undertrack signatures. When winds are included, the undertrack profile is not geometrically undertrack, as seen from the ground intersection location in the Y direction. The X component of the wind is in the direction of actual flight path, while the Y component of the wind is in the negative Y direction. When the offtrack ground signature is computed in the presence of winds, the ray path is a combination of azimuthal angle and wind effects. For example, in the figure, for about 8000 m from the aircraft altitude, the effect of azimuth on the ray path location in the Y direction is mostly countered by the wind velocity. However, as the propagation distance increases toward the ground, the azimuthal effect overcomes the wind effect because of lower wind velocities at lower altitudes (see Table 1), and the ground intersection location is much smaller compared with the no-wind offtrack case.

Table 2 Ground ray intersection and propagation times

Case	Azimuth	Heading	X range, m	Y range, m	Propagation time, s
No winds	0.0	0.0	11,418.71	0.0	62.59
No winds	0.0	45.0	8,074.24	8,074.24	62.59
No winds	0.0	90.0	0.0	11,418.71	62.59
No winds	30.0	0.0	13,643.58	10,261.22	74.68
Winds	0.0	0.0	13,844.17	−6, 222.80	61.337
Winds	0.0	−90.0	3,071.46	−16, 311.43	60.358
Winds	0.0	180.0	−9, 062.06	−6, 452.71	64.28
Winds	0.0	90.0	3,317.56	6,834.346	66.757
Winds	30.0	0.0	18,259.62	3,203.44	77.05
Winds	30.0	−90.0	11,775.93	−17, 972.03	67.57
Winds	30.0	180.0	−9, 336.0	−17, 108.25	72.82
Winds	30.0	90.0	——	——	——

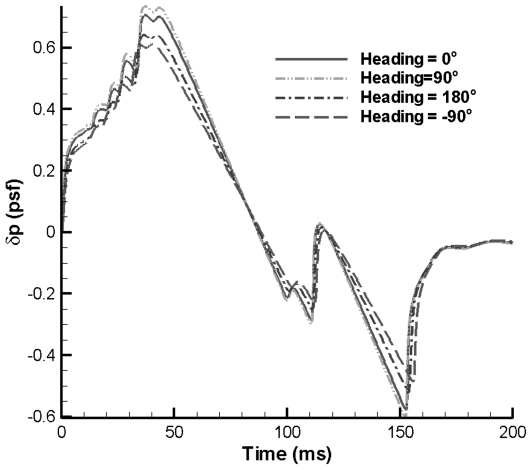

Fig. 9 Effect of heading angle.

The ground intersection locations of the ray paths along with propagation times are listed in Table 2. For the cases where winds are absent, the propagation times do not vary with heading angle. However, the ranges in the Cartesian coordinates change according to the heading angle. For the no-winds case, propagation toward an offtrack location increases the propagation times as well as the ground ray intersection ranges. In the case of winds, the ranges and propagation times vary significantly with the heading and azimuthal angles. For a heading of 90° and an azimuthal angle of 30°, the atmospheric refraction causes the rays to be refracted until they no longer intersect the ground after a certain distance. Thus, this heading and azimuthal combination is beyond the boom cutoff. Ray paths thus play an important role in signature evolution when computing the sonic boom ground footprints. The ground intersections and offtrack signatures will be helpful in path planning exercises at a future date.

B. Effect of Heading on Ground Signatures

If atmospheric winds are assumed to be absent, then the aircraft heading does not have an effect on the predicted sonic boom ground signatures. In reality, however, winds are inevitable in the atmosphere. Winds, being vectors, have a significant impact on the sonic boom footprint when considered along with the aircraft heading angle, making the ray paths asymmetric with respect to the aircraft heading. The comparison of the ground signatures with different heading angles is given in Fig. 9. When the heading is either 0 or 90°, the wind direction components are aiding the flight speed, resulting in a faster signature propagation toward the ground. In addition, because of higher wave normal velocities, the ray path angles with respect the horizontal plane are steeper (from Snell's law); therefore, the ray paths to the ground intersection are shorter. On the other hand, for the other heading angles plotted in the figure, the wind at flight altitude is working against the flight direction. This leads to shallower ray angles moving more slowly toward the ground and, because of the lower ray path angles compared with the 0 and 90° heading angles, the ray paths are longer until the ground intersection. The higher wave normal velocities for the cases with wind components aiding the propagation process cause an increase in pressure magnitudes based on the Blokhintzev invariant. The

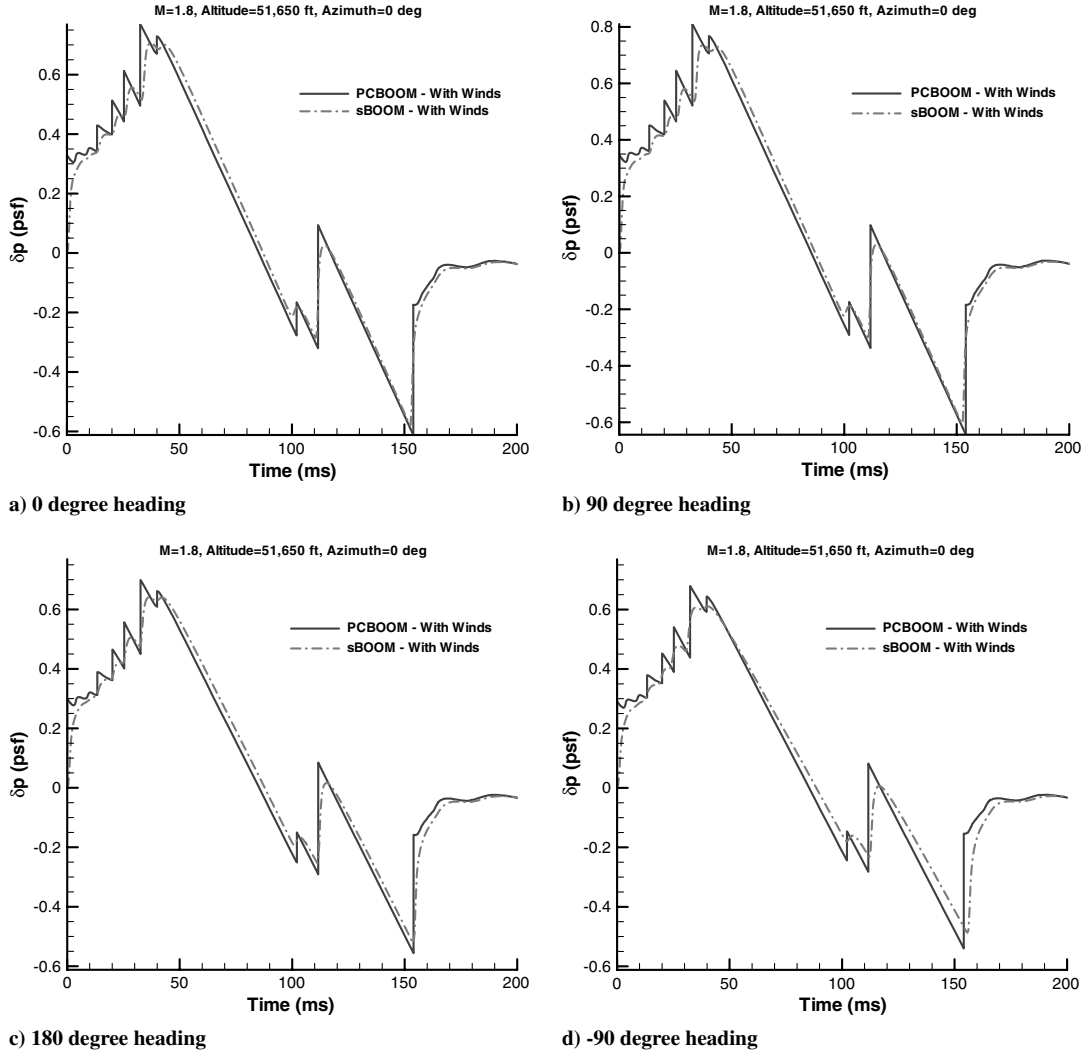

a) 0 degree heading

b) 90 degree heading

c) 180 degree heading

d) -90 degree heading

Fig. 10 Comparison of undertrack ground signatures with winds at different heading angles.

reducing headwinds closer to the ground drag the ray paths farther forward, making the paths longer with shallower intercept angles at the ground. This allows additional attenuation of the signatures seen for heading angles −90 or 180° compared with 0 or 90°. The shock locations are well aligned, irrespective of the heading angle; however, the magnitude changes appreciably.

Finally, Figs. 10 and 11 compare the sBOOM undertrack and offtrack signatures with PCBOOM in the presence of winds at different heading directions. All sBOOM signatures match very well with PCBOOM with respect to shock locations and magnitudes. The rounding differences can be attributed to the modeling of advanced atmospheric propagation effects not included in the PCBOOM propagation process.

One limitation of using sBOOM compared with PCBOOM is the longer computation time needed for calculating the sonic boom footprints. On an average, each PCBOOM run requires approximately about 0.15 s, while each sBOOM run usually requires about 3 s on a 64-bit Intel Xeon Dual-Core 2.8 GHz processor. This time calculation is based on using 20,000 sampling points during propagation. Using more or less sampling points would change the run times appropriately. On an average, the time to run sBOOM is about 20–25 times slower than PCBOOM. The primary reason for this is the high sampling rate of the waveform used in the sBOOM propagation process. Since the sampling rate cannot be reduced too much without affecting accuracy, one possible avenue of load alleviation during an multidisciplinary analysis and optimization evaluation of a geometry is to run sBOOM simultaneously with another independent analysis that requires more time to run than sBOOM. Nonetheless, the additional time to run sBOOM is probably needed to ensure that the loudness metrics do not involve any empiricism.

V. Conclusions

A new sonic boom prediction tool has been developed. This method solves the augmented Burgers equation numerically. By including effects such as nonlinearity, molecular relaxation, and thermoviscous absorption into the propagation process, the thickness of the shocks is predicted analytically. In addition, the signatures are inherently smooth. This avoids artificial smoothing and empirical shock thickening during loudness calculation. Undertrack and offtrack ground signatures may be calculated in the presence or absence of winds to provide a sonic boom carpet of any vehicle concept. This is a useful tool in the design of supersonic aircraft. Future work will include enhancing this capability as needed in design exercises.

Acknowledgments

The work by the author was supported by the NASA project entitled “Multi-Fidelity Conceptual Design Process,” under NASA contract number NNL08AA00B. The author would like to thank Robin O. Cleveland for assistance during the early phases of development of the boom prediction capability. Thanks are also due to Gulfstream Aerospace, particularly to Joe Salamone and Kenrick Waithe, for providing a case for validation and for sharing their thoughts on the Burgers equation propagation process.

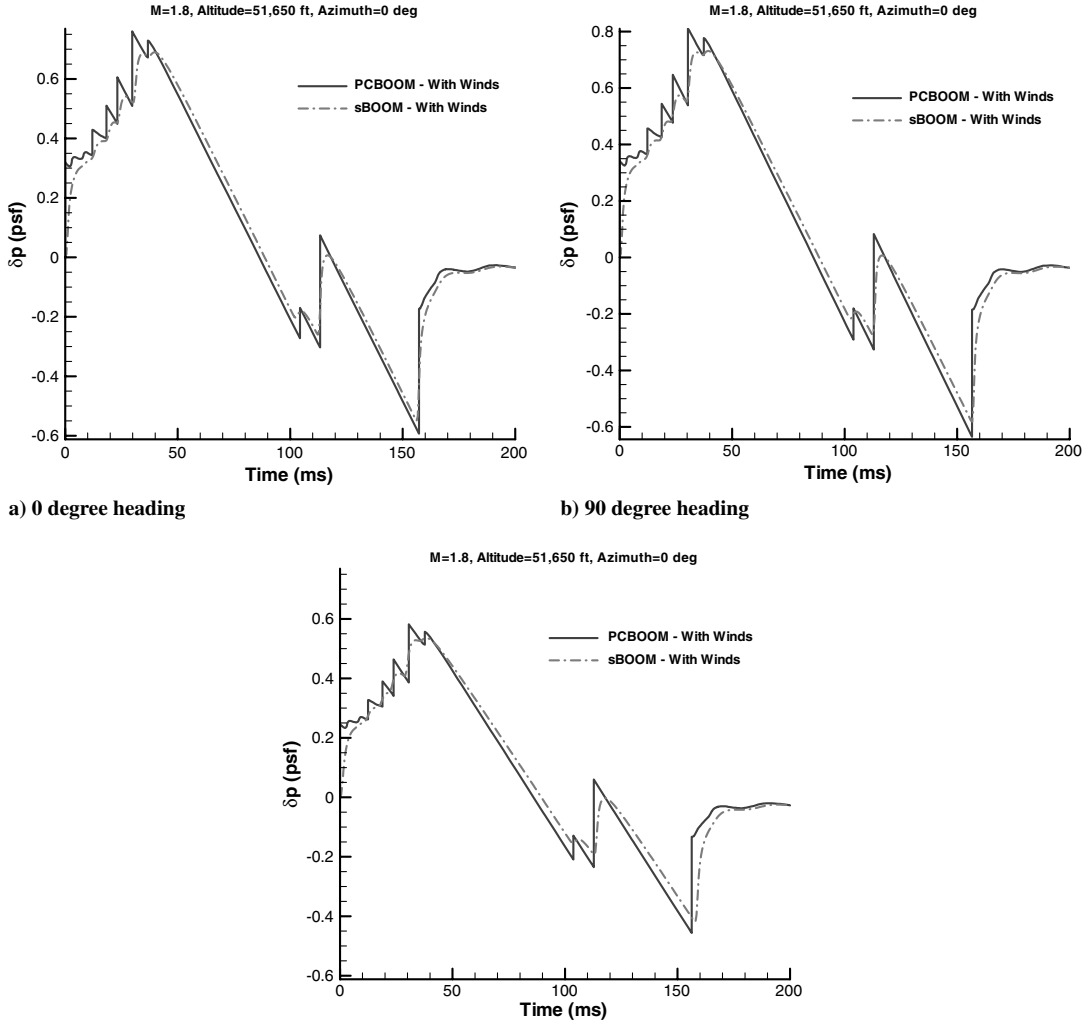

a) 0 degree heading

b) 90 degree heading

c) 180 degree heading

Fig. 11 Comparison of offtrack ground signatures with winds at different heading angles.

References

[1] Whitham, G., "The Flow Pattern of a Supersonic Projectile," *Communications on Pure and Applied Mathematics*, Vol. 5, No. 3, 1952, pp. 301–347.
doi:10.1002/cpa.3160050305.doi:

[2] Hayes, W. D., "Brief Review of Basic Theory: Sonic Boom Research, NASA SP147, 1967, pp. 3–7.

[3] Hayes, W. D., Haefeli, R. C., and Kulsrud, H. E., "Sonic Boom Propagation in a Stratified Atmosphere with Computer Program," NASACR 1299, April 1969.

[4] Thomas, C., "Extrapolation of Sonic Boom Pressure Signatures by the Waveform Parameter Method," NASA, TN D-6832, June 1972.

[5] Plotkin, K. J., "Computer Models for Sonic Boom Analysis: PCBoom4, CABoom, BooMap, COR- Boom," Wyle Rept. WR 02-11, Arlington, VA, June 2002.

[6] Seebass, R., and George, A., "Sonic Boom Minimization," *Journal of the Acoustical Society of America*, Vol. 51, No. 2, 1972, pp. 686–694.
doi:10.1121/1.1912902

[7] George, A. R., "Lower Bounds for Sonic Booms in the Midfield," *AIAA Journal*, Vol. 7, No. 8, 1969, pp. 1542–1545.
doi:10.2514/3.5429

[8] George, A. R., and Seebass, R., "Sonic Boom Minimization Including Both Front and Rear Shock Waves," *AIAA Journal*, Vol. 9, No. 10, 1971, pp. 2091–2093.
doi:10.2514/3.6478

[9] Seebass, R., and Argrow, B., "Sonic Boom Minimization Revisited," AIAA Paper 1998-2956, June 1998.

[10] Darden, C., "Sonic Boom Minimization with Nose-Bluntness Relaxation," NASA Langley Research Center, TP 1348, Hampton, VA, Sept. 1979.

[11] Plotkin, K. J., Rallabhandi, S. K., and Li, W., "Generalized Formulation and Extension of Sonic Boom Minimization Theory for Front and Aft Shaping," AIAA Paper 2009-1052, Jan. 2009.

[12] Robinson, L. D., "Sonic Boom Propagation Through an Inhomogeneous Windy Atmosphere," Ph.D. Thesis, Univ. of Texas at Austin, Austin, TX, 1991.

[13] Cleveland, R. O., "Propagation of Sonic Booms Through a Real, Stratified Atmosphere," Ph.D. Thesis, Univ. of Texas at Austin, Austin, TX, 1995.

[14] Pilon, A. R., "Spectrally Accurate Prediction of Sonic Boom Signals," *AIAA Journal*, Vol. 45, No. 9, 2007, pp. 2149–2156.
doi:10.2514/1.28159

[15] Li, W., Shields, E., and Geiselhart, K., "A Mixed- Fidelity Approach for Design of Low- Boom Supersonic Aircraft," AIAA Paper 2010-0845, Jan. 2010.

[16] George, A., and Plotkin, K. J., "Sonic Boom Waveforms and Amplitudes in a Real Atmosphere," *AIAA Journal*, Vol. 7, No. 10, Oct. 1969, pp. 1978–1981.
doi:10.2514/3.5491

[17] Randall, D. G., "Sonic Bang Intensities in a Stratified Still Atmosphere," *Journal of Sound and Vibration*, Vol. 8, No. 2, 1968, pp. 196–214.
doi:10.1016/0022-460X(68)90227-7

[18] Onyeonwu, R. O., "The Effects of Wind and Temperature Gradients on Sonic Boom Corridors," Univ. of Toronto Inst. for Aerospace Studies TN 168, Toronto, Oct. 1971.

[19] Hayes, W. D., and Runyan, H. L., "Propagation of Sonic Boom Through a Stratified Atmosphere," *Proceedings of the Analytical Methods in Aircraft Aerodynamics Symposium*, NASA SP-228, 1970, pp. 229–244.

[20] Plotkin, K. J., "Review of Sonic Boom Theory," Proceedings of the 12th AIAA Aeroacoustics Conference, AIAA Paper 1989-1105, April 1989.

[21] Campbell, R. L., Carter, M. B., Deere, K. A., and Waithe, K. A., "Efficient Unstructured Grid Adaptation Methods for Sonic Boom Prediction," AIAA Paper 2008-7327, Aug. 2008.

[22] Frink, N. T., Pirzadeh, S., Parikh, P., Pandya, M., and Bhat, M., "The NASA Tetrahedral Unstructured Software System," *The Aeronautical Journal*, Vol. 104, No. 1040, 2000, pp. 491–499.

[23] Stevens, S., "Perceived Level of Noise by Mark VII and Decibels," *Journal of the Acoustical Society of America*, Vol. 51, No. 2, 1972, pp. 575–601.
doi:10.1121/1.1912880

[24] Makino, Y., and Kroo, I. M., "Robust Objective Functions for Sonic-Boom Minimization," *Journal of Aircraft*, Vol. 43, No. 5, 2006, pp. 1301–1306.
doi:10.2514/1.19442